The Abdus Salam
International Centre for Theoretical Physics

United Nations
Educational, Scientific
and Cultural Organization

International Atomic
Energy Agency

H4.SMR/1775-30

"8th Workshop on Three-Dimensional Modelling of
Seismic Waves Generation, Propagation and their Inversion"

25 September - 7 October 2006

Deep structure of the Afro-Arabian hotspot by S receiver functions

Lev Vinnik

Institute of Physics of the Earth
Moscow, Russia

Deep structure of the Afro-Arabian hotspot by S receiver functions

L. P. Vinnik
Institute of Physics of the Earth, Moscow, Russia

V. Farra
Institut de Physique du Globe de Paris, Paris, France

R. Kind
GeoForschungsZentrum Potsdam, Potsdam, Germany

Received 25 January 2004; revised 7 April 2004; accepted 11 May 2004; published 10 June 2004.

[1] We investigated deep structure of the Afro-Arabian hotspot by using recordings from Geoscope seismograph station ATD. The records are processed with the S receiver function technique, which allows a detection of Sp converted phases from the upper mantle discontinuities. The seismic data reveal two unusual discontinuities. The discontinuity at a depth of 160 km beneath the Gulf of Aden corresponds to the onset of melting. If the water content in olivine is around 800 $H/10^6$Si, melting at this depth requires a temperature close to 1550°C, about 120°C higher than the average. Another remarkable discontinuity is found at a depth of 480 km, where S velocity drops with depth by about 0.2 km/s. This can be the head of another plume which is trapped in the mantle transition zone. *INDEX TERMS:* 7203 Seismology: Body wave propagation; 7218 Seismology: Lithosphere and upper mantle; 8121 Tectonophysics: Dynamics, convection currents and mantle plumes. **Citation:** Vinnik, L. P., V. Farra, and R. Kind (2004), Deep structure of the Afro-Arabian hotspot by S receiver functions, *Geophys. Res. Lett.*, *31*, L11608, doi:10.1029/2004GL019574.

1. Introduction

[2] We investigate deep structure of one of the largest and most intriguing hotspots, which occupies Afar, the Ethiopian plateau, the Red Sea and the southern and western Arabia (Figure 1). Tomographic images [*Ritsema et al.*, 1999] reveal in the upper mantle of the study region a prominent low-velocity anomaly. The waveforms of higher modes of Rayleigh waves indicate that the low velocity body beneath Afar and western Arabia extends to a depth of 660 km [*Debayle et al.*, 2001].

[3] Our study is conducted with the aid of the S receiver function technique [*Farra and Vinnik*, 2000]. A similar study of two ancient large igneous provinces (LIPs) was conducted earlier [*Vinnik and Farra*, 2002]. Receiver function techniques present a powerful tool for mapping structure of the upper mantle. However, in the P receiver function techniques that are used in many recent studies, possible arrivals of Pds (P-to-S converted phases from a depth d) are masked by reverberation of crustal origin. The slowness of the crustal phases is close to that of the Pds phases from the uppermost mantle, and a separation of them is problematic. In the S receiver functions crustal reverberation arrives later than the mantle S-to-P converted phases, a major advantage over the other receiver function techniques.

0094-8276/04/2004GL019574$05.00

2. Method

[4] To detect the Sdp phases, the 3-component seismogram is decomposed into P, SV, T and M components [*Farra and Vinnik*, 2000]. The SV axis corresponds to the principal S particle motion direction in the wave propagation plane. The P axis is perpendicular to SV in the same plane and is optimal for detecting Sdp phases. The T axis is perpendicular to SV and P. The M axis corresponds to the principal motion direction of the S wave in the T-SV plane and is characterized by the angle θ with the SV axis. The P components are deconvolved by their respective M components. Combined processing of the deconvolved P components of many seismic events yields P_c and P_s, that present the response of the Earth's medium in a vicinity of the seismograph station to the excitation by SV and T components of S, respectively. The excitation of the P component by the T is possible in the presence of azimuthal anisotropy.

[5] The solution for either P_c or P_s is equivalent to stacking of the deconvolved P components with weights depending on their respective θ and variance of noise. The procedure of record processing involves evaluation of the standard error of the amplitude of the stack, which is practically the RMS value of the random noise which is present in the stack. To account for the difference in slowness between the Sdp phases and the parent phases, the estimates of P_c and P_s are obtained by stacking the deconvolved P components with moveout time corrections. The corrections are obtained as a product of differential slowness (the difference in slowness between the signal and the parent phase) and differential distance (the difference between the epicentral distance of the event and the average distance).

[6] Search for the optimum velocity model is conducted by comparing the stack of the actual receiver functions with its synthetic analogues. Synthetic seismograms are generated with a reflectivity technique [*Fuchs and Mueller*, 1971; *Kind*, 1985]. The signals in the actual P_c are formed mainly by those seismograms that are stacked with the highest weights. In the modeling satisfactory results are obtained with the synthetics at the epicentral distances of the high-weight seismograms by assuming for them a shallow focal

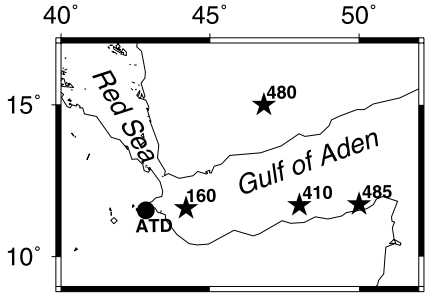

Figure 1. Map of the study region. Stars with numbers are piercing points of the Sdp rays at depths (in km) indicated by the numbers. The calculations were conducted for the S wave at a distance of 83° in the back azimuth of 90° and at a distance of 90° in the back azimuth of 45°.

mechanism with a strong radiation of S and SKS phases in the direction of the receiver. We assume that the converted phases are generated by the S wave at epicentral distances less than 90° and by SKS phase at larger distances. Accordingly, the synthetic receiver functions are calculated separately for the S and SKS phases. A typical modeling experiment is demonstrated below.

[7] The results for station LVZ in Fennoscandia (Figure 2) are representative for many other stations. The traces in Figure 2a are obtained by stacking 151 recordings in a distance range from 66° to 105° with the average around 83°. The wave field contains two Sdp phases that are detected with confidence near −4 s and −52 s at a differential slowness of 0 s/deg and 0.8 s/deg, respectively. Both are with negative polarity which means that the S velocity is higher at the underside of the respective discontinuity. These phases are generated at the Moho and "410 km" discontinuity, respectively. Amplitude of S410p phase normalized to the amplitude of SV (0.027) is 7 times larger than the standard error (0.004). The stack contains an arrival at a time around 28.5 s (marked by question mark). It can be interpreted as a superposition of the Sdp phase from the Lehmann discontinuity and of a sidelobe of the Sdp phase from the Moho. The synthetic stack for standard IASP91 model [*Kennett and Engdahl*, 1991] reproduces the main features of the observed wave field (Figure 2b).

3. Data and Results for Station ATD

[8] If compared with Figure 2a, the data of Geoscope station ATD (see Figure 1) are more complicated (Figure 3). The available recordings are divided into two groups with the average back azimuths around 90° and 45°. The number of recordings in the groups is 86 and 48, respectively. The average epicentral distances are around 83° and 90°. In the first azimuth (Figure 3a) we recognize arrivals with negative polarity from the Moho (at −3 s) and from "410 km" discontinuity (at −60 s). What makes these data anomalous, are two additional phases: the first is at a time of −23 s with a slowness of −0.4 *s*/°; the second is at a time of −70 s with a slowness of 0.8 *s*/°. Amplitudes of both (around 0.03) are several times larger than the standard error (0.005). Weighting of the individual receiver functions is optimal for the interval between −70 s and −20 s, but not for the interval between −100 s and −80 s, where the stack is more noisy.

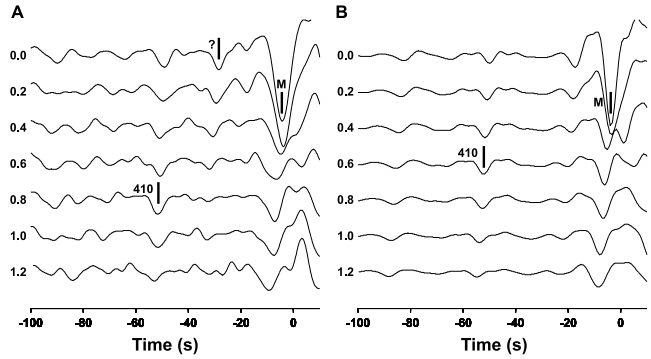

Figure 2. Actual (a) and synthetic (b) P_c traces for station LVZ. The numbers on the left are values of differential slowness in *s*/°. The arrivals of the Sdp phases are marked. Note that P_c is free from the S wave motion that arrives at a time 0. The synthetic seismograms are computed for IASP91 model [*Kennett and Engdahl*, 1991] by the method described in the text.

The first phase (at a time of −23 s) could be a sidelobe of the Sdp phase from the Moho boundary. However, then the amplitude of the sidelobe should be larger than the actual one in the deconvolved S by an order of magnitude. Moreover, this is incompatible with the slowness of the first phase (−0.4 s/deg), that is very different from the slowness of the

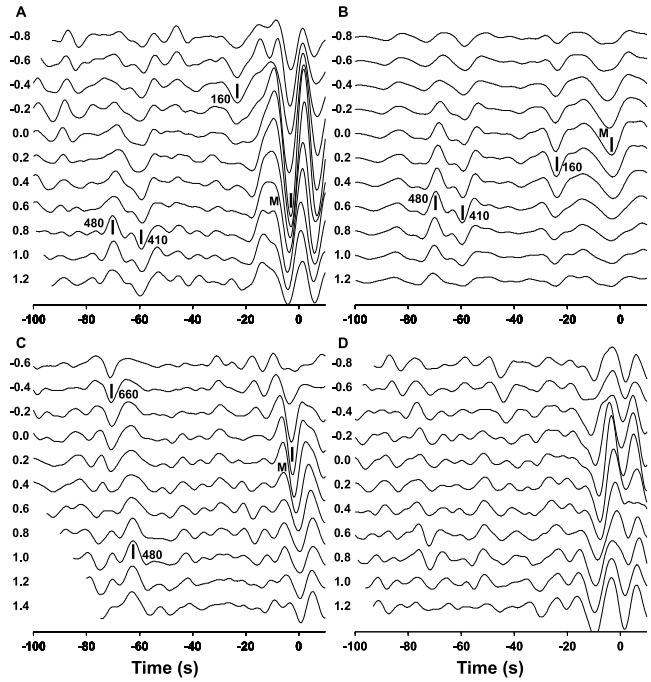

Figure 3. Data for station ATD. a - the same as (a) in Figure 2, but for 86 recordings of ATD with the average back azimuth around 90° and average epicentral distance of 83°. b - synthetic P_c traces for the back azimuth of 90°; the S velocity model is shown in Figure 4. c - the same as in (a) but for 48 recordings with the average back azimuth around 45° and the average epicentral distance around 90°. d - the same as in (a) but for P_s; note that in the P_s traces there is no seismic signal at a time of −23 s, which is present in (a).

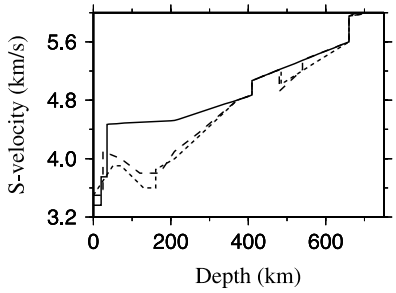

Figure 4. S velocity models: short and long dash lines are for ATD, back azimuths of 90° and 45°, respectively; solid line is for IASP91 [*Kennett and Engdahl*, 1991].

phase from the Moho (0.0 s/deg). Positive polarity of the phase at −70 s implies that it is converted from a discontinuity with a lower S velocity at the underside.

[9] The first-order features of the data in Figure 3a are reproduced by the synthetics (Figure 3b) for the S velocity model in Figure 4. The model was found by assuming two low velocity regions: one in the uppermost mantle and the other in the transition zone. The parameters of the model were adjusted to make them compatible with the observations. To suppress effects of the sidelobes in the synthetics, the transition from the crust to the mantle in the model is smoothed. As a result, the synthetic stack in the interval from −15 s to 10 s looks different from the actual data, but this interval is of a minor significance for our study. The phases at −23 s and −70 s correspond to the discontinuities at 160 and 485 km.

[10] The reduction of S velocity in our model up to 22% relative to standard model [*Kennett and Engdahl*, 1991] at 100–150 km depths is required by the observed travel time of S410p. This reduction is consistent with the values that were inferred from the phase velocities of surface waves in western Arabia [*Knox et al.*, 1998]. In the modeling we assume the standard depth of "410 km" boundary. Heating of the upper mantle should be accompanied by downwarping of the discontinuity by 10 km per 140°C [*Katsura and Ito*, 1989]. This would reduce the differential travel time between P410s and P660s phases in the P receiver functions, but this effect is not observed [*Chevrot et al.*, 1999; *Nyblade et al.*, 2000; *Vinnik et al.*, 2003]. Moreover, the piercing points of S410p are located far from the central region (Figure 1). If, in spite of these arguments, the discontinuity is depressed by 10 km, this would result in a travel time anomaly of around −1.5 s out of the observed −8 s. Then the maximal reduction of S velocity in the model would be 18% instead of 22%. Obviously the effect is small.

[11] Our modeling is based on the assumption of lateral homogeneity of the upper mantle in the corridor sampled by the waves. This assumption is justified by a similarity of the differential slownesses of the actual phases and their synthetic analogues. The largest discrepancy (0.6 s/deg) is observed in the slowness of the signal that arrives at −23 s. This can be explained by a tilt of the respective discontinuity on the order of a few degrees.

[12] In the second azimuth (Figure 3c) we recognize the signal from the Moho (at −2.6 s), a phase with positive polarity at −62 s, and a phase with negative polarity at −73.5 s. Amplitudes of these phases are several times larger than the standard error (0.005). If compared with the first group, the second group contains relatively few events at distances less than 90° and many events at larger distances. As a result the theoretical amplitude of S410p phase in the second group is much lower than in the first group, and this may explain the absence of the S410p in Figure 3c. The difference in the epicentral distances is also the reason for the large amplitude of S660p phase in Figure 3c and its practical absence in Figure 3a. The signal with positive polarity in Figure 3c is similar to that in Figure 3a: the difference in time (−62 s versus −70 s) is caused mainly by the difference in the average epicentral distance.

[13] The data in Figure 3c testify that the signal with positive polarity is not a random feature, and it cannot be interpreted as a sidelobe of the S410p phase, that is missing. The phase at −62 s in Figure 3c corresponds to the top of a low velocity layer at a depth of 480 km (Figure 4). The phase at −73.5 s can be interpreted as a superposition of two phases: SKS phase converted to P from "660 km" discontinuity and S phase converted from the bottom of the low velocity layer at a depth of 540 km. Average S velocity in the uppermost mantle in the second azimuth is higher than in the first azimuth. This is an effect of azimuthal anisotropy: the fast direction of anisotropy in a vicinity of ATD is close to 50° [*Vinnik et al.*, 1989; *Barruol and Hoffmann*, 1999].

4. Discussion and Conclusions

[14] The boundary at a depth of 160 km could be interpreted as an effect of a transition from an anisotropic layer to the isotropic medium underneath the layer. Then a signal of comparable amplitude would be present in P_s in Figure 3d which is not the case. Alternatively the discontinuity may correspond to the onset of melting of peridotite. For a likely content of water in olivine 800 $H/10^6$Si, melting at a depth of 160 km requires a temperature of 1550° [*Hirth and Kohlstedt*, 1996], about 120°C higher than the average. This value is among the highest proposed for the hotspots [*Anderson*, 2000]. In the P receiver functions P160s phase arrives at the time of crustal reverberation, and a detection of it is impossible.

[15] Our analysis suggests that the low-velocity anomaly beneath Afar and neighboring regions may consist of two separate bodies with a lateral extent of a few hundred kilometers (Figure 1). This structure is clearly different from the mushroom-shaped plumes of laboratory simulations. Temperature anomaly in the lower body, as derived from the velocity anomaly, is about 500°C, a few times higher than in the upper body. The Afro-Arabian hotspot belongs to a small group of 'primary' ones originating, most likely, in the thermal boundary layer in the lower mantle [*Courtillot et al.*, 2003]. Relative to the rest of the mantle, this layer is probably composed of a different, intrinsically more dense material [*Kellogg et al.*, 1999]. The fate of a thermal plume arising from this layer is predetermined by the buoyancy flux that depends on intrinsic density and thermal expansion [*Albers and Christensen*, 1996]. If the thermal boundary layer is compositionally stratified, plumes or their portions generated at larger depths may have lower

buoyancy in spite of the higher temperature. The deep low velocity body may present a low buoyancy portion of the plume that is trapped in the mantle transition zone.

[16] The reversal in the S velocity profile at a depth of 480 km could be detected in P receiver functions, but the region, where the deep low velocity layer may reside (Figure 1), is devoid of seismograph stations, and at present this test is impossible. Future studies will show if this layer can be found elsewhere.

[17] **Acknowledgments.** Digital recordings were provided by IRIS DMC. L. Vinnik was supported by RFBR grant 01-05-64243, by GFZ Potsdam and by Alexander-von-Humboldt foundation. The authors appreciate comments from Jeroen Ritsema and an anonymous reviewer.

References

Albers, M., and U. R. Christensen (1996), The excess temperature of plumes rising from the core-mantle boundary, *Geophys. Res. Lett.*, *23*, 3567–3570.

Anderson, D. L. (2000), The thermal state of the upper mantle: No role for mantle plumes, *Geophys. Res. Lett.*, *27*, 3623–3626.

Barruol, G., and R. Hoffmann (1999), Upper mantle anisotropy beneath the Geoscope stations, *J. Geophys. Res.*, *104*, 10,774–20,757.

Chevrot, S., L. Vinnik, and J.-P. Montagner (1999), Global scale analysis of the mantle Pds phases, *J. Geophys. Res.*, *104*, 20,203–20,219.

Courtillot, V., A. Davaille, J. Besse, and J. Stock (2003), Three distinct types of hotspots in the Earth mantle, *Earth Planet. Sci. Lett.*, *205*, 295–308.

Debayle, E., J.-J. Leveque, and M. Cara (2001), Seismic evidence for a deeply rooted low-velocity anomaly in the upper mantle beneath northeastern Afro/Arabian continent, *Earth Planet. Sci. Lett.*, *193*, 423–436.

Farra, V., and L. Vinnik (2000), Upper mantle stratification by P and S receiver functions, *Geophys. J. Int.*, *141*, 699–712.

Fuchs, K., and G. Mueller (1971), Computation of synthetic seismograms with the reflectivity method and comparison with observations, *Geophys. J. R. Astron. Soc.*, *23*, 417–433.

Hirth, G., and D. L. Kohlstedt (1996), Water in the oceanic upper mantle: Implications for rheology, melt extraction and the evolution of the lithosphere, *Earth Planet. Sci. Lett.*, *144*, 93–108.

Katsura, T., and E. Ito (1989), The system Mg_2SiO_4 – Fe_2SiO_4 at high pressures and temperatures: Precise determination of stabilities of olivine, modified spinel, and spinel, *J. Geophys. Res.*, *94*, 15,663–15,670.

Kellogg, L. H., B. H. Hager, and R. D. van der Hilst (1999), Compositional stratification in the deep mantle, *Science*, *283*, 1881–1884.

Kennett, B. L. N., and E. R. Engdahl (1991), Traveltimes for global earthquake location and phase identification, *Geophys. J. Int.*, *105*, 429–465.

Kind, R. (1985), The reflectivity method for different source and receiver structures, *J. Geophys.*, *58*, 146–152.

Knox, R. B., A. A. Nyblade, and C. A. Langston (1998), Upper mantle S velocities beneath Afar and western Saudi Arabia from Rayleigh wave dispersion, *Geophys. Res. Lett.*, *25*, 4233–4236.

Nyblade, A. A., R. B. Knox, and H. Gurrola (2000), Mantle transition zone thickness beneath Afar: Implications for the origin of the Afar hotspot, *Geophys. J. Int.*, *142*, 615–619.

Ritsema, J., H. J. van Heijst, and J. H. Woodhouse (1999), Complex shear wave velocity structure imaged beneath Africa and Iceland, *Science*, *286*, 1925–1928.

Vinnik, L., and V. Farra (2002), Subcratonic low-velocity layer and flood basalts, *Geophys. Res. Lett.*, *29*(4), 1049, doi:10.1029/2001GL014064.

Vinnik, L. P., V. Farra, and B. Romanowicz (1989), Azimuthal anisotropy in the Earth from observations of SKS at Geoscope and NARS broadband stations, *Bull. Seismol. Soc. Am.*, *79*, 1542–1558.

Vinnik, L., M. Ravi Kumar, R. Kind, and V. Farra (2003), Super-deep low-velocity layer beneath the Arabian plate, *Geophys. Res. Lett.*, *30*(7), 1415, doi:10.1029/2002GL016590.

V. Farra, Department de Sismologie, CNRS UMR 7580, Institut du Physique du Globe de Paris, 4 Place Jussieu, F-75252 Paris cedex, France. (farra@ipgp.jussieu.fr)

R. Kind, GeoForschungsZentrum Potsdam (GFZ), Telegrafenberg, D-14473 Potsdam, Germany. (kind@gfz-potsdam.de)

L. P. Vinnik, Institute of Physics of the Earth, Bolshaya Grouzinskaya 10, 123995 Moscow, Russia. (vinnik@dubna-2.scgis.ru)